Signatures of Proprioceptive Control in *C. elegans* Locomotion

Supplementary Materials

Jack E. Denham, Thomas Ranner and Netta Cohen

S1. A CONTINUUM NEUROMECHANICAL MODEL

S1.1. Mechanical model

We use Cohen and Ranner's continuum mechanical model to capture the characteristic low Reynolds number undulatory movement of *C. elegans*.[1] In this model, the nematode's body is represented by a thin viscoelastic shell. Aside from the elasticity and viscosity of the shell, the model worm is subject to internal pressure, external forces from the environment, modelled using resistive force theory, and active muscle forcing.

The high internal pressure in *C. elegans* is represented as a line tension p along this midline and is chosen such that the midline is inextensible (with length fixed at 1 mm from head to tail). Internal pressure helps maintain the worm's shape and relaxes the body back to a straight configuration in the absence of muscle activation.

Bending due to active muscle force is represented by a torque acting on the midline of the body. As we show below, this torque may be expressed as a *preferred curvature* $\beta = \beta(u,t)$ along the body midline; here, $\beta(u,t)$ has units of curvature, u denotes the position along the midline of the body (from 0 in the head to 1 in the tail) and t denotes time. Thus, $\beta(u,t)$ will vary along the body coordinate and in time. The preferred curvature is analogous to a time-changing rest (or preferred) length in a spring, whose response is proportional to its displacement as captured by Eq. (S2). We adopt a convention in which positive and negative values of β correspond to dorsal and ventral excitation respectively. The body curvature, $\kappa = \kappa(u,t)$, is generated by the active moment $\beta(u,t)$ which in turn follows the muscle activation $A(u,t)$.

Finally, the resistive environmental drag forces are decomposed into two forces acting in directions normal and tangential to the body,

$$\boldsymbol{F}_{\text{env}} = K_\nu v_\nu \boldsymbol{\nu} + K_\tau v_\tau \boldsymbol{\tau} \tag{S1}$$

with corresponding drag coefficients $K_\nu \geq K_\tau$ acting along the normal, $\boldsymbol{\nu}$, and tangential,

$\boldsymbol{\tau}$, directions, respectively; here, v_ν and v_τ denote the normal and tangential components of speed of a point along the body. The balance of forces is summarized as follows:

$$\boldsymbol{F}_{\text{env}} - \frac{(p\boldsymbol{\tau})_u}{|\boldsymbol{x}_u|} + \frac{1}{|\boldsymbol{x}_u|}\left(\frac{EI_2}{|\boldsymbol{x}_u|}(\kappa-\beta)_u\boldsymbol{\nu} + \frac{\eta I_2}{|\boldsymbol{x}_u|}\kappa_{tu}\boldsymbol{\nu}\right)_u = 0\,, \tag{S2}$$

where $\boldsymbol{x}$ denotes a coordinate of a point along the body (in the lab frame) and the subscripts t and u denote partial derivatives with respect to t and u (along the midline of the worm), respectively. Equation (S2) allows us to seamlessly translate between units of torque and body curvature. The function I_2 represents the second moment of area

$$I_2(u) = \frac{\pi}{2}\left[\left(R(u) + \frac{r_{\text{cuticle}}}{2}\right)^4 - \left(R(u) - \frac{r_{\text{cuticle}}}{2}\right)^4\right], \tag{S3}$$

where R, the radius of the body, varies along the body and is defined as

$$R(u) = \bar{R}\,\frac{2\sqrt{(\epsilon+u)(\epsilon+1-u)}}{1+2\epsilon} \tag{S4}$$

for small ϵ (which sets the width of the body at the head and tail ends). Zero force and zero torque are enforced at the boundaries, such that $\beta = \kappa$ at both ends of the body.

Nondimensionalization

A detailed description of the non-dimensionalization is given by Cohen and Ranner (2017)[1]. Briefly, the equations are recast in non-dimensional form and typical parameters are imposed in a regime of interest. These include geometrical quantities (the length and second moment of area of the worm), a time scale, estimated material properties of the body (the Young's modulus and internal viscosity) and external drag coefficients.

Estimates of the Young's modulus of the worm vary from $O(\text{kPa})$ to $O(100\,\text{MPa})$. For purposes of non-dimensionalization, here we adopt a mid-range value of $E = 5\,\text{MPa}$.[1] (Note that this value differs from our simulation default value of $E = 100\,\text{kPa}$; see Table 1, and further discussion below.) Using a time scale and drag coefficients matching the undulation period of *C. elegans* in agar-like conditions and corresponding drag coefficients (Table S1), yields a reduced model in which the internal viscosity is negligible. Hence, the non-dimensional model equation can be expressed in terms of only two dimensionless parameters

$$K = \frac{K_\nu}{K_\tau}\,, \qquad\qquad e = \frac{I\,T_0}{L^4}\,\frac{E}{K_\tau}\,, \tag{S5}$$

	Description	Label	Value
Geometric constants			
	Body length	L	$1\,\mathrm{mm}$
	Cuticle width	r_{cuticle}	$0.5\,\mu\mathrm{m}$
	Maximum radius along body	$\bar{R}$	$40\,\mu\mathrm{m}$
Muscle constants			
	Muscle timescale	τ_m	0.1 s
	Curvature amplitude	β_0	$10\ \mathrm{mm}^{-1}$
Nondimensionalization			
	Young's modulus	E	$5\,\mathrm{x}\,10^6\,\mathrm{Pa}$
	Undulation period (agar)	T_0	$3.3\,\mathrm{s}$
	Tangential drag coefficient (agar)	K_τ	$3.2\ \mathrm{kg\,m^{-1}\,s^{-1}}$
	Normal drag coefficient (agar)	K_τ	$128\ \mathrm{kg\,m^{-1}\,s^{-1}}$
Feed-forward control			
	Feed-forward wavelength	λ_f	$0.6\,\mathrm{mm}$
	Feed-forward period	T_f	$2\,\mathrm{s}$
Proprioceptively-driven control			
	Proprioceptive threshold	θ	3
	Proprioceptive range	δ	0.5

TABLE S1: Parameters used in model.

where $I = 2\pi\bar{R}^3 r_{\mathrm{cuticle}}$, yielding the dimensionless model equation for the balance of forces

$$Kv_\nu \boldsymbol{\nu} + v_\tau \boldsymbol{\tau} - \frac{(p\boldsymbol{\tau})_u}{|\boldsymbol{x}_u|} + \frac{e}{|\boldsymbol{x}_u|}\left(\frac{I_2}{|\boldsymbol{x}_u|}(\kappa-\beta)_u\boldsymbol{\nu}\right)_u = 0. \tag{S6}$$

In this non-dimensional formulation, all variables are also non-dimensional (e.g., $\kappa \to \kappa L$). For notational simplicity, we continue to use the same symbols for these non-dimensional entities except where otherwise stated (or units given). The non-dimensional model is solved using a finite element method with 128 mesh points.[1] Its key advantages for our purposes here are seamless integration with neural and muscular control, numerical stability and high computational efficiency.

S1.2. Neuromechanical coupling

Model muscles

Cohen and Ranner's model[1] uses instantaneous forcing $\beta(u,t)$ to generate body bending. In other words, that model lacks an explicit representation of muscles and neurons. Here, we include a minimal muscle model, whose input can be viewed as a current input from the nervous system and whose output is the muscle torque $\beta(u,t)$, which acts directly on the viscoelastic shell (since nematode body wall muscles are tethered to the cuticle of the animal). Rather than discrete body wall muscles, our model uses a continuous muscle forcing along the ventral and dorsal sides, approximating the effect of ventral and dorsal muscles. Muscles respond to neural activation with a muscle time scale τ_m, and the combined activation of ventral and dorsal muscles translates to an effective torque that acts on the midline of the body, given here in dimensional form as

$$\tau_m \frac{d\beta}{dt} = -\beta + \beta_0 A \,, \tag{S7}$$

where $A = A(u)$ represents a neural activation or muscle input, $\beta = \beta(u,t)$ is the torque experienced by the midline, and β_0 is the amplitude of the preferred curvature and dictates the amplitude of undulations (or maximal curvature κ, see Eq. (S6)).

Central pattern generated control

Here, we consider a minimal model in which the action of this circuit on the muscles can be captured by continuous unit amplitude oscillations with an imposed period, T_f, and undulation wavelength, λ_f, propagating from head to tail. Thus, the input to the muscles is given by travelling sine wave

$$A(u,t) = \sin(2\pi u L/\lambda_f - 2\pi t/T_f) \,, \tag{S8}$$

given, again, in dimensional form. Our choice of this model is motivated precisely by its simplicity, to serve as a minimal model of feed-forward (open loop) control and as a basis for comparison with our own model of feedback-driven control and with future models of neural control, whether driven by feed-forward or feedback control.

Proprioceptively driven control

We assume proprioceptively generated control relies exclusively on feedback from the shape of the body of the nematode. The *C. elegans* forward locomotion motor circuit consists of command interneurons that innervate motor neurons along the ventral nerve cord. Ventral motor neurons innervate ventral body wall muscles and dorsal motor neurons innervate dorsal body wall muscles (Fig. 1*a*). B-type motor neurons are the primary excitatory motor neurons implicated in forward locomotion.[2] Here, we model B-type motor neurons as bistable elements, following Boyle *et al.* (2012)[3] and inspired by electrophysiological recordings of bistable RMD head motor neurons.[4] In our continuous representation of the body, the state of ventral (VB) and dorsal (DB) motor neurons at a point u along the body is given by $V^{\mathrm{V}}(u), V^{\mathrm{D}}(u) \in \{0, 1\}$, respectively.

In our simplified representation of the circuit, only B-type neurons are represented explicitly. The activation of B-type motor neurons is determined by two components: (i) current inputs from other neurons in the locomotion neural circuit and (ii) a dynamic proprioceptive current. A tonic input from the AVB command interneurons, and VD to VB inhibition are included implicitly. The former is treated as a constant and can therefore be absorbed into the switching threshold θ. VD to VB inhibition is treated as a reset[3] that ensures VB and DB neurons are always in antiphase (when VB is on, DB is off and *vice versa*). For a neuron at position u, the proprioceptive input current is typically modelled as the stretch of one side of the body (ventral or dorsal) relative to a rest length. It is easy to show that in our fixed radius geometry, this measure of stretch can be reformulated as a measure of curvature, which allows us to use our representation of the midline of the body. In fact, during forward locomotion the *C. elegans* undulation wavelength and amplitude typically scale with body size (for example during development),[5] suggesting that any sensing of length changes along the body scale similarly (in other words measuring relative rather than absolute length changes). Conveniently, the non-dimensional curvature κ exactly captures such length-invariant deformation due to stretch along the body. Accordingly, here, the proprioceptive input current $I_\kappa(u)$ is given by the mean body curvature over a specified proprioceptive range, represented as a fraction of the body length, $\Delta(u)$:

$$I_\kappa(u) = \frac{\int_u^{u+\Delta(u)} \kappa(u')|\boldsymbol{x}_u(u')|\,\mathrm{d}u'}{\int_u^{u+\Delta(u)} |\boldsymbol{x}_u(u')|\,\mathrm{d}u'}. \tag{S9}$$

We note that this is equivalent to having formulated the proprioceptive response in terms of the dimensional curvature and having non-dimensionalized the result. The input current represents the effective stretch of each side of the body arising in the (non-dimensional) mechanical model. Here, we adopt a convention whereby a positive (negative) range corresponds to a posterior (anterior) receptive field, and where positive curvatures κ, a positive proprioceptive input current and a positive preferred curvature β all correspond to dorsal bending, whereas negative values correspond to ventral bending. Anteriorly facing processes are found in A-type motor neurons of the ventral nerve cord and have been implicated in backward locomotion.[2,6,7]

When the proprioceptive input $I_\kappa(u)$ exceeds the proprioceptive threshold θ (Table S1), the dorsal neuron will switch off and the ventral one on. When the input falls below some threshold (here, taken as $-\theta$ for symmetry) the dorsal neuron will switch on and the ventral one off. We implicitly assume synchrony of DB and VD, and similarly of VB and DD (see Fig. 1*a*). Neuronal state switching is then given by

$$\begin{aligned} &\text{If} \quad I_\kappa(u) > \theta\,, \quad \text{then} \quad \begin{cases} V^{\mathrm{D}}(u) \to 0 \\ V^{\mathrm{V}}(u) \to 1\,; \end{cases} \\ &\text{If} \ I_\kappa(u) < -\theta\,, \quad \text{then} \quad \begin{cases} V^{\mathrm{D}}(u) \to 1 \\ V^{\mathrm{V}}(u) \to 0\,. \end{cases} \end{aligned} \tag{S10}$$

Here, the proprioceptive range $\Delta(u)$ is set to δ for $u \in [0, 1-\delta]$ (in the anterior of the body when $\delta = 0.5$ (Table S1)) and decreases linearly as $1-u$ in the posterior $u \in [1-\delta, 1]$, i.e. $\Delta(u) = \min(\delta, 1-u)$. The activation thresholds are set to effective (non-dimensional) curvatures of $\pm\theta = \pm 3$. By imposing anti-phase activation, the state at position u along the body reduces to the difference between the dorsal and ventral activation

$$A(u) = V^{\mathrm{D}}(u) - V^{\mathrm{V}}(u) = \pm 1.$$

This activation $A(u)$ then feeds into Eq. (S7) to drive the muscles.

Model Code

The model code is publicly available and can be found at the following address:
`https://bitbucket.org/leedswormlab/curve-worm-royal-society-paper`

S2. COMPUTING KINEMATIC PARAMETERS

For convenience, simulation inputs and outputs are converted to dimensional units, as appropriate. All simulations were performed for 60 seconds using integration time steps of 0.3 ms for feed-forward control and 0.03 ms for proprioceptive control. The transients in some simulations were negligible (<1 s) but others varied significantly with model parameters. In all kinematic analysis, we truncated the transient, thus limiting our analysis to periodic activity.

Frequency: The period of undulations, T, was computed from curvature kymograms. For a given point along the body, the period was defined as the mean time interval between zero crossing of the body curvature $\kappa(u,t)$ at $u = 0.125$ (from negative to positive values). In coordinated locomotion, the period of undulation does not depend on the position along the body. The frequency of undulations is given by $f = 1/T$.

Wavelength: In our proprioceptive model (as in experimental observations), the undulation wavelength increases along the body (from head to tail). We defined wavelength as the distance along the midline of the body spanning an entire cycle of body curvatures.[8] This distance along the body is the physiologically meaningful entity and can therefore be extracted from the postural dynamics of the worm. (The conventional *wavelength* is given by the straight line connecting the corresponding two points along the body.) Note that for sufficiently dilute (low viscosity) environments, the wavelength is longer than the length of the body. We computed wavelength by calculating the gradient of the curvature $\kappa(u,t)$ as a function of body coordinate u and time t within a section of the body. Towards the tip of the tail the value of the wavelength changes. This may be due to a combination of boundary effects and decreasing proprioceptive range. We therefore exclude the tail and tip of the head in our measure of wavelength which we define as

$$\lambda = T \frac{\partial\kappa/\partial u}{\partial\kappa/\partial t} \tag{S11}$$

over the region $u \in (0.1, 2/3)$. A small amount of filtering of the curvatures ensured that the derivatives are well approximated using a finite difference. An average was taken across u and time t using a histogram mode with logarithmically distributed bins.

Speed: Speed was computed by tracking the midpoint of the nematode's body ($u = 0.5$) over time, and performing a straight line fit over the midpoint trajectory to remove side-to-

side displacement arising from the undulatory movement. The speed was then defined as the distance travelled along the straight line over the corresponding time interval.

Thrust: To gain insight into the propulsive thrust, we considered the progress made per undulation. Thrust was therefore defined as speed/frequency and normalized by the body length to yield a dimensionless measure (corresponding to 1-slip in the notation of Gray and Lissmann (1964)[9]).

Neuromechanical Phase Lag: To calculate the phase lag $\phi(u,t)$, we took the Hilbert transform of the torque, $\beta(u,t)$, and curvature, $\kappa(u,t)$, separately using MATLAB's inbuilt `hilbert` function. Unwrapping the angles yielded monotonically increasing phases along the body for each point in time, $\phi_\beta(u,t)$ and $\phi_\kappa(u,t)$. The neuromechanical phase lag $\phi(u,t)$ was defined as the time averaged difference $\phi(u,t) = \phi_\kappa(u,t) - \phi_\beta(u,t)$. The corresponding time lags were obtained by normalizing by the angular frequency, $2\pi f$.

S3. SUPPLEMENTARY RESULTS

Supplementary Figure captions

Figure S1:
Simulations of proprioceptively driven control with anteriorly facing proprioceptive feedback. Simulation parameters as in Table S1 except for the proprioceptive range, set to $\delta = -0.5$ such that $\Delta(u) = \max(-u, \delta)$ and integration limits in Eq. (S9) updated accordingly. (a) Backward locomotion in low K environment. (b) Backward locomotion in a high K environment. Reversing the polarity of the proprioceptive current to polarize rather than depolarize the neurons in response to stretch, or else to depolarize in response to contraction rather than stretch reinstates forward locomotion.

Figure S2:
Undulation frequency, wavelength and speed, obtained from simulation results of proprioceptively driven forward locomotion with default parameter values for the neural control, in a variety of Newtonian media and with different body Young's moduli. The results are taken from Fig. 2 of the main paper and replotted here as a function of the dimensional tangential drag coefficient. Frequency, wavelength and speed all increase with body stiffness but fall with increasing fluid viscosity. The expected range of gait modulation depends on material properties of the body.

Figure S3:
Extended simulation results of proprioceptively driven forward locomotion in eight different viscoelastic fluids, subject to different proprioceptive thresholds. All other simulation parameters are the default values (Table S1). Figure 3a in the main paper shows results for four of the eight conditions shown here (a,b and f). During coordinated locomotion, the frequency determines the speed indicating that the proprioceptive threshold effect on thrust is negligible (c–e).

Figure S4:
Extended simulation results of proprioceptively driven forward locomotion in eight different

viscoelastic fluids, subject to different proprioceptive ranges. All other simulation parameters are the default values (Table S1). Figure 3*b* in the main paper shows results for four of the eight conditions shown here (a,b and f). (a) Undulation frequency falls with increasing proprioceptive range across all environments tested. (b) The sensitivity of the undulation wavelength grows with increasing proprioceptive range. Here, considerable gait modulation requires an effectively large proprioceptive range of 40-50% of the body. (c) Significant thrust and (d) speed require an effectively non-local proprioceptive range. The most efficient locomotion is obtained for a maximal thrust, which declines for long proprioceptive ranges (>50% of the body), indicating that speed is not fully determined by the undulation frequency (e).

Figure S5:

Neuromechanical phase and time lags for different control circuits. (a–b) Neuromechanical time lags (as distinct from phase lags) under (a) feed-forward and (b) proprioceptive control, corresponding to results from Fig. 4 from main paper. (c) Neuromechanical time lags and (d) corresponding phase lags, obtained from simulations with a proprioceptive range of $\delta = 0.2$ and a range of Young's moduli. The phase lag is now clamped for $u \in [0, 0.8]$ before increasing near the tail. The increase in lag is more substantial for lower values of Young's modulus. (e) Fixing the Young's modulus at the default value (100 kPa) and varying the proprioceptive range, δ. The phase clamping breaks down consistently around $u = 1 - \delta$.

S3.1. Anterior proprioception leads to backward locomotion

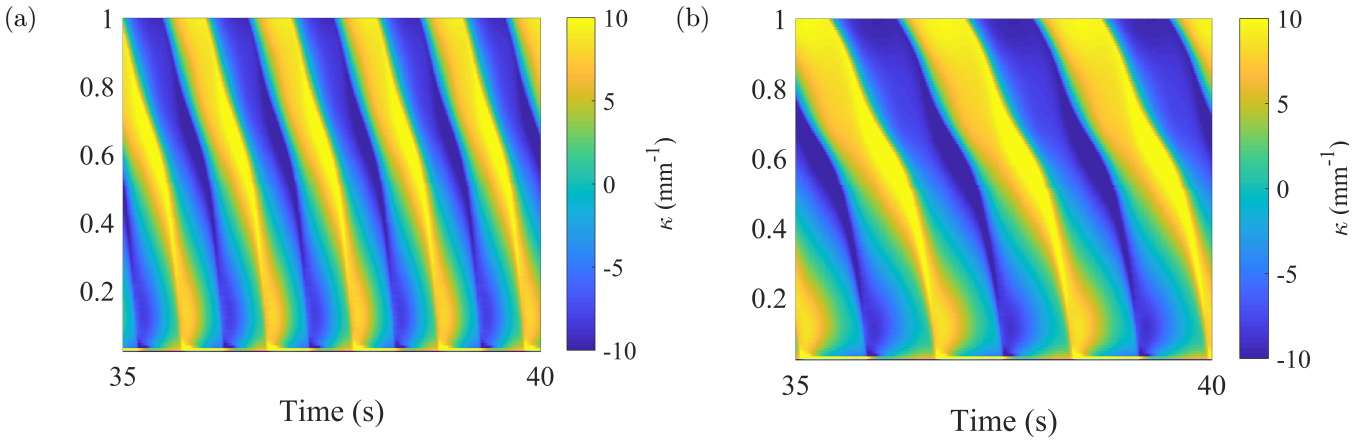

FIG. S1:

S3.2. Proprioceptive feedback couples undulatory kinematics to biomechanical parameters

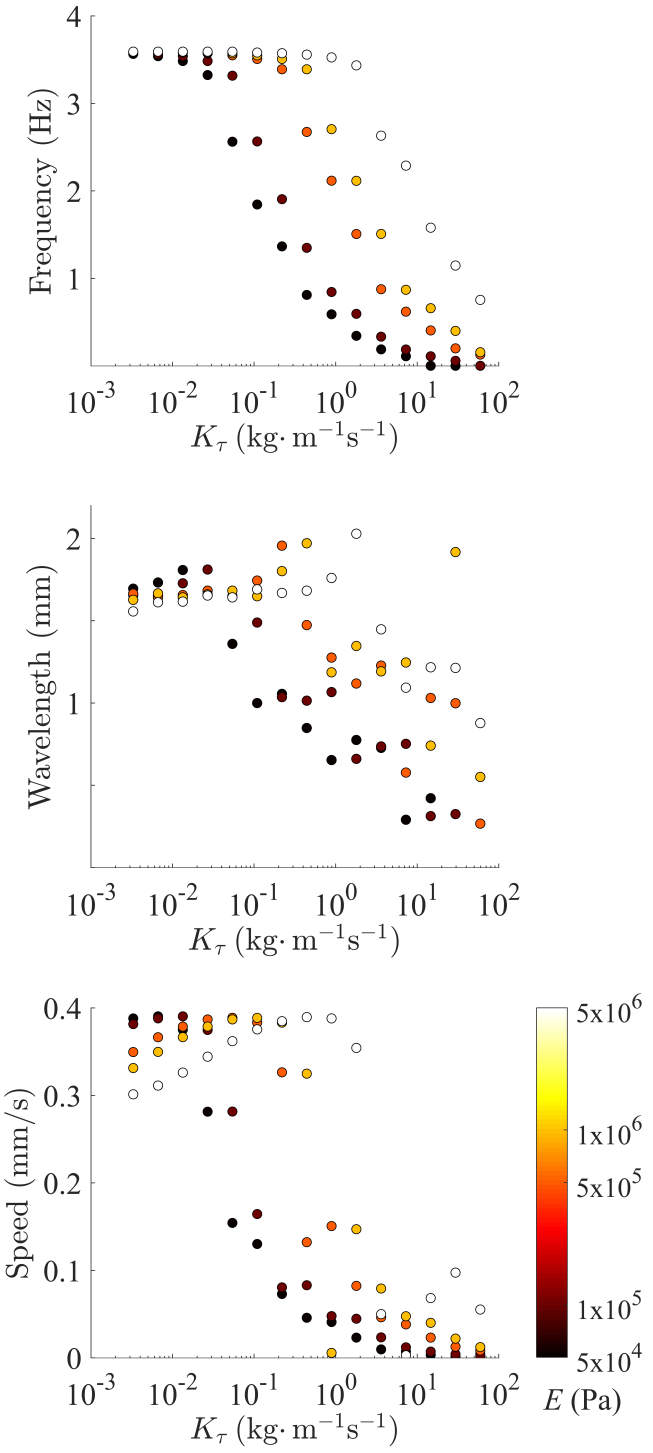

FIG. S2:

S3.3. The kinematics of forward locomotion depends on the proprioceptive threshold

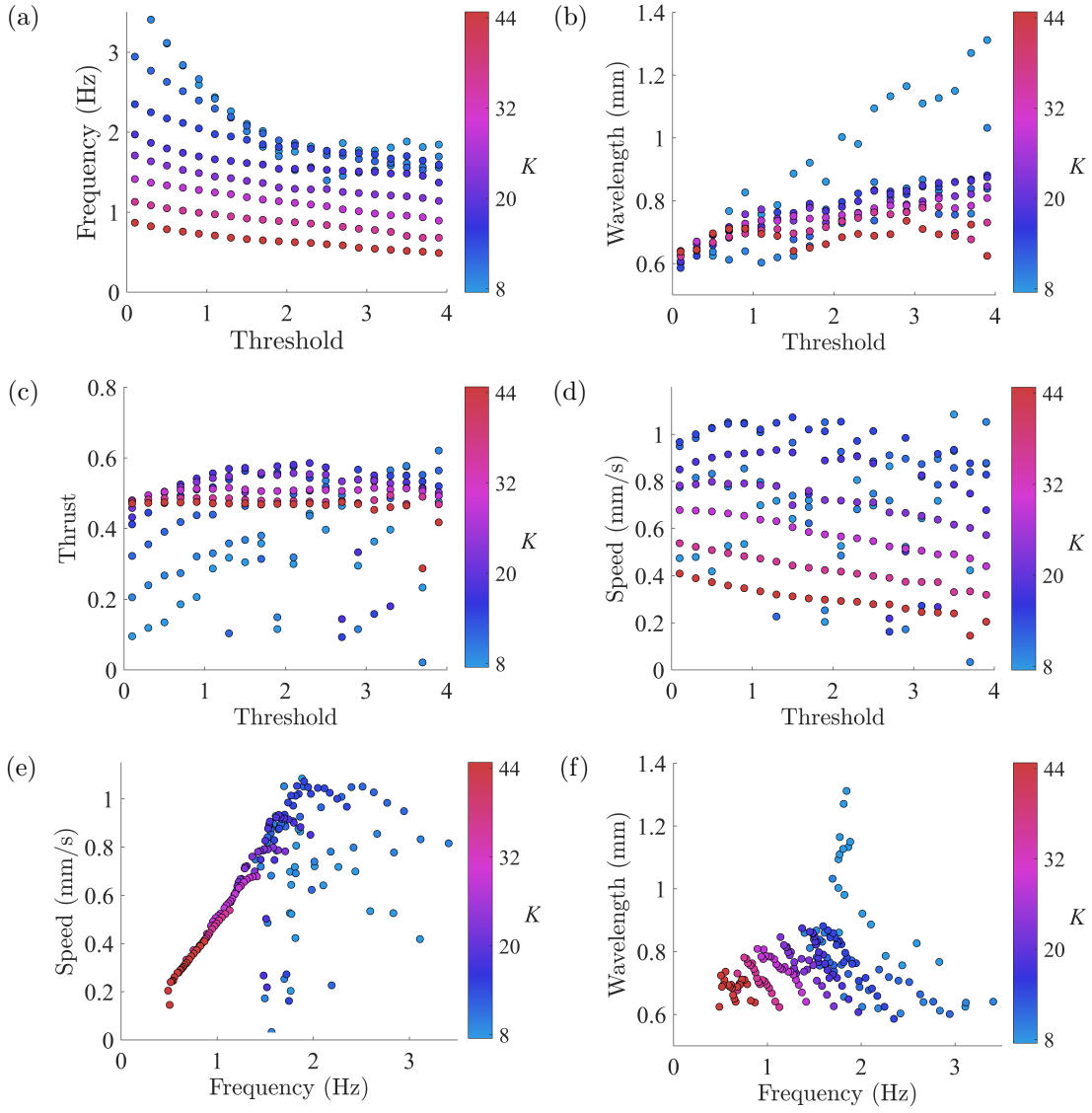

FIG. S3:

S3.4. The kinematics of forward locomotion depends on the effective proprioceptive range

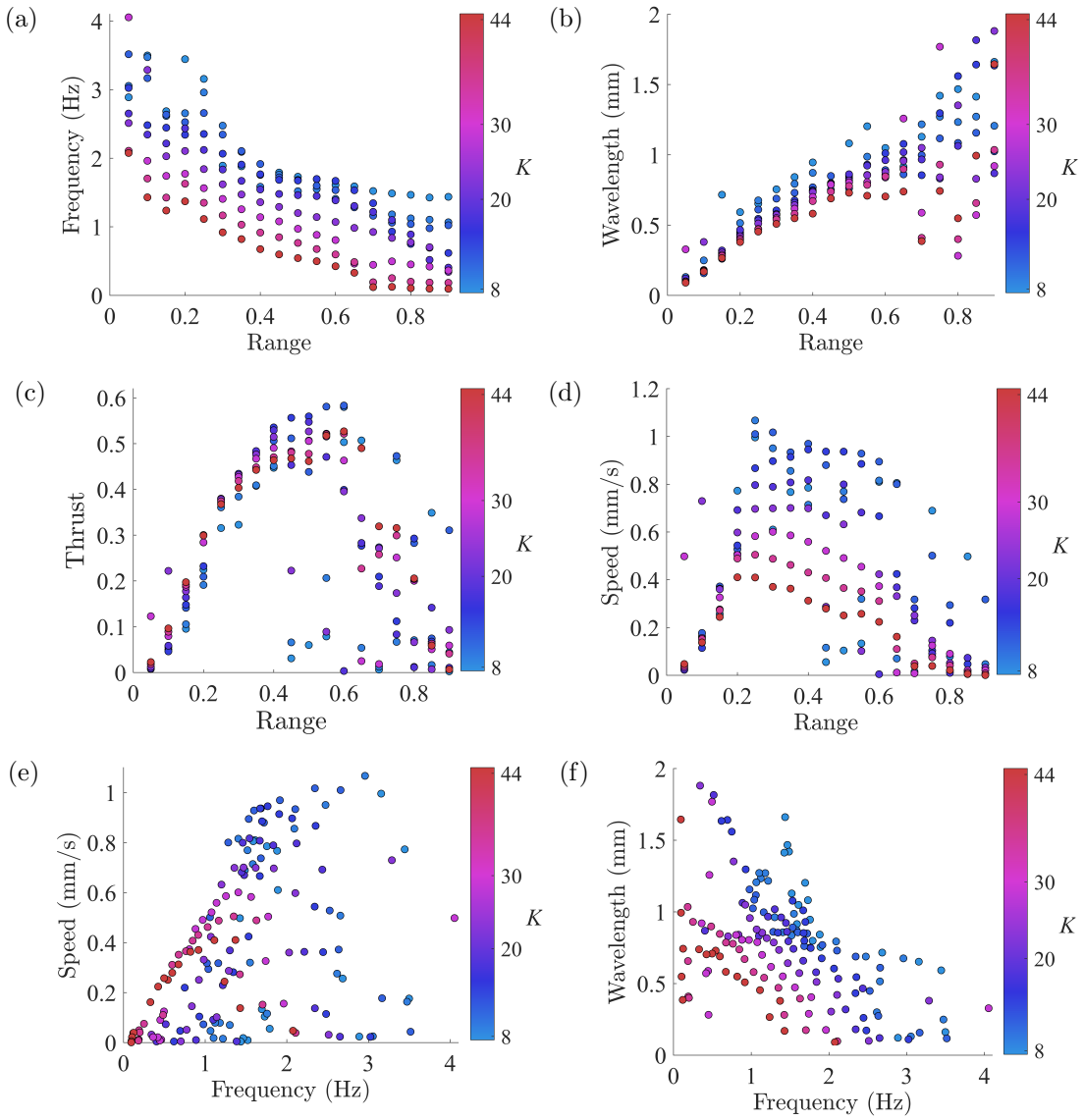

FIG. S4:

S3.5. Reducing proprioceptive range confirms anterior phase lag clamping under feedback control

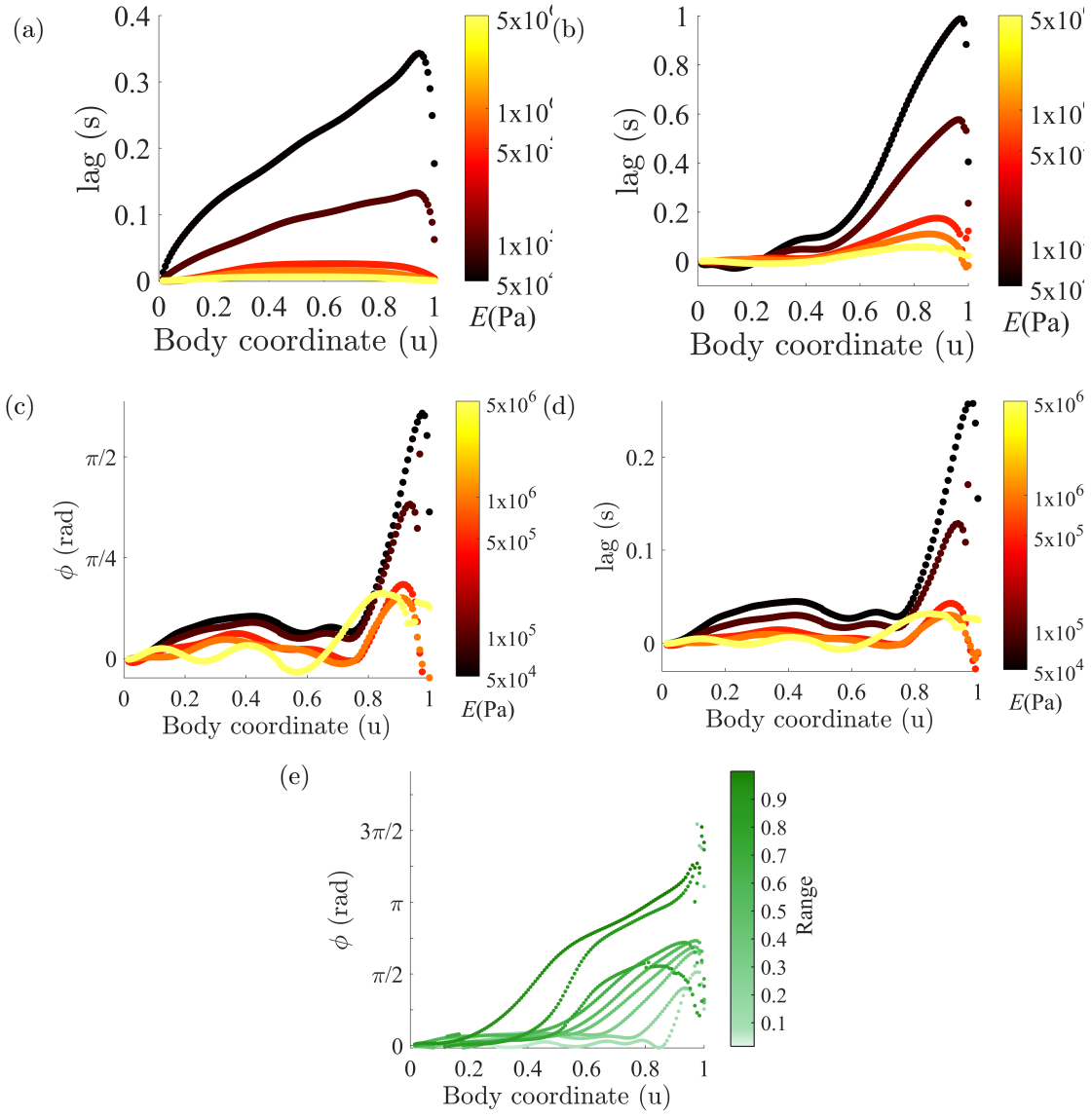

FIG. S5:

REFERENCES

[1]N. Cohen and T. Ranner. A new computational method for a model of *C. elegans* biomechanics: Insights into elasticity and locomotion performance. *arXiv e-prints 1702.04988*, 2017.

[2]M. Chalfie, J. Sulston, J. White, E. Southgate, J. Thomson, and S. Brenner. The neural circuit for touch sensitivity in *Caenorhabditis elegans*. *Journal of Neuroscience*, 5(4):956–964, 1985.

[3]J. H. Boyle, S. Berri, and N. Cohen. Gait modulation in *C. elegans*: an integrated neuromechanical model. *Frontiers in Computational Neuroscience*, 6:10, 2012.

[4]J. E. Mellem, P. J. Brockie, D. M. Madsen, and A. V. Maricq. Action potentials contribute to neuronal signaling in *C. elegans*. *Nature Neuroscience*, 11(8):865–867, 2008.

[5]J. Karbowski, C. J. Cronin, A. Seah, J. E. Mendel, D. Cleary, and P. W. Sternberg. Conservation rules, their breakdown, and optimality in *Caenorhabditis* sinusoidal locomotion. *Journal of Theoretical Biology*, 242(3):652–669, 2006.

[6]J. White, E. Southgate, J. Thomson, and S. Brenner. The structure of the nervous system of the nematode *Caenorhabditis elegans*. *Philos. Trans. R. Soc. Lond. B, Biol. Sci.*, 314: 1–340, 1986.

[7]S. Gao, S. A. Guan, A. D. Fouad, J. Meng, T. Kawano, Y.-C. Huang, Y. Li, S. Alcaire, W. Hung, Y. Lu, *et al.* Excitatory motor neurons are local oscillators for backward locomotion. *eLife*, 7:e29915, 2018.

[8]S. Berri, J. H. Boyle, M. Tassieri, I. A. Hope, and N. Cohen. Forward locomotion of the nematode *C. elegans* is achieved through modulation of a single gait. *HFSP Journal*, 3(3): 186–193, 2009.

[9]J. Gray and H. W. Lissmann. The locomotion of nematodes. *Journal of Experimental Biology*, 41(1):135–154, 1964.